Intense femtosecond laser filamentation: physics and applications

S. L. Chin[a], W. Liu[a], S. A. Hosseini[a], Q. Luo[a], F. Théberge[a], N. Aközbek[b], A. Becker[c], V. P. Kandidov[d] and O. G. Kosareva[d]
[a]*Centre d'Optique, Photonique et Laser (COPL) & Département de Physique, de Génie Physique et d'Optique Université Laval, Québec, Qc. G1K 7P4, Canada.*
[b]*Timedomain Corp., Huntsville, Alabama, USA*
[c]*Max-Planck Institute for the Physics of Complex System, Dresden, Germany*
[d]*International Laser Center, Department of Physics, Moscow State University, Moscow, Russia*

(Received 25 July 2005)

Powerful femtosecond laser pulses propagate in an apparent form of filaments in all transparent optical media. This universal nonlinear phenomenon is currently an interesting topic of research at the forefront of applied physics with a lot of challenging physics and potential applications.

I. SLICE-BY-SLICE SELF-FOCUSING LEADS TO FILAMENTATION

Fundamentally, the physics of filamentation is based upon Kerr self-focusing. It is well known that the optical Kerr will give rise to a positive intensity dependent nonlinear Kerr index of refraction $\Delta n = n_2 I$ (where n_2 is the second order nonlinear index coefficient and *I*, the intensity). Assuming a Gaussian transverse intensity distribution beam, the total index of refraction at the central part of the pulse is higher than that at the outer zone. The velocity of propagation being c/n (where *c* is the velocity of light in vacuum and *n* the total index of refraction: $n = n_0 + \Delta n_{Kerr}$, n_0 being the linear index of refraction), the central part of the beam will propagate slower than the outer zone. Thus, the wave front of the pulse will curve forward (concave) as it propagates; i.e. it is focusing more and more strongly during the propagation. This is called self-focusing. Self-focusing is a threshold process. It will take place if the power of a continuous wave (CW) Gaussian laser beam is higher than the critical power P_c for self-focusing [1]:

$$P_c = 3.77\lambda^2 / 8\pi n_0 n_2 . \qquad (1)$$

In Eq. (1), λ is the wavelength. This is the so-called whole beam steady state Kerr self-focusing. In principle, so long as there is a non-uniform intensity distribution in the wave front of the pulse, and the peak power is high enough, self-focusing will occur.

However, in the case of a powerful femtosecond laser pulse, it is what we call by 'slice by slice' self-focusing that is taking place during the propagation [2,3]. The temporal shape of the laser pulse is considered to be an intensity or power envelope defined by the Poynting vector. It is visualized as subdivided into many thin intensity or power slices in time (or in space along the propagation axis). We assume that the pulse is Gaussian in space transverse to the propagation axis *z* and in time (i.e. in the propagation direction) and its peak power is much higher than the critical power for self-focusing. The central slice of the pulse will self-focus at a distance z_f from the beginning of the propagation in the medium given by [1]:

$$z_f = \frac{0.367 k a_0^2}{\left\{\left[(P/P_c)^{1/2} - 0.852\right]^2 - 0.0219\right\}^{1/2}}, \qquad (2)$$

as if this slice were a CW beam. In equation (2), *k* and a_0 are the wave number and the radius of the beam profile at $1/e$ level of intensity, respectively and *P* is the peak power of the slice. The most powerful slice at the center of the pulse will self-focus first. Before the slice self-focuses towards a singularity, the intensity is already high enough to ionize the medium through multiphoton/tunnel ionization in gas media or multiphoton excitation from valance band to the conductive band in condensed matters followed by a few cycles of cascade ionization. The resulting weak plasma density (~10^{14} to 10^{16} cm^{-3} in air [4-8] and 5 to 6×10^{19} cm^{-3} in condensed matters [9,10]) would be sufficient to de-focus the focusing. The highest intensity that this self-focusing slice would reach is thus limited due to the balance between self-focusing in the neutral and self-defocusing in the self-generated weak plasma. We call this intensity clamping [11-13]. During the propagation, the repeated processes of Kerr self-focusing in the neutral and self-defocusing in the self-generated weak plasma of the various slices in the front part of the pulse result in an extended series of hot spots along the propagation axis; i.e. filamentation [2,14-16]. Successive slices from the back part of the pulse will self-focus into the plasma of the previous self-focal region. This interaction with the plasma will naturally de-focus these slices and no self-focus is formed with these slices.

The above picture/interpretation is based upon the results of numerical simulations of the pulse propagation

in a transparent medium under the condition of the so-called single filament (see for example, ref. [2,17,18]. Essentially, every slice, be it the one from the front or the back, after being de-focused by the self-induced plasma in the self-focal region will 'release' its energy back into the pulse outside the self-focal zone. This constitutes the idea of background field/energy reservoir first proposed by the Arizona group led by Moloney [15,19] and later expanded by Kandidov and Kosareva *et al*. [20]. The energy at the self-focus comes always from the outside reservoir in the sense of slice-by-slice self-focusing. It is not the self-focus that self-channels through the medium as if there is nothing outside the central filament. There are many experimental proof of such a slice-by-slice self-focusing or background reservoir picture [2,3,21-23]**.** Fig. 3 shows a set of experimental measurement of the appearance of the filamentation process. This will be discussed further in section III.

II. CHIRPED WHITE LIGHT LASER AND CONICAL EMISSION

The interaction of the high intensity in the self-focal regions with the neutral gas and with the plasma results in the modulation of the phase of the pulse; i.e. self-phase modulation (SPM) (See for example, [24]). The consequence is spectral broadening towards both the red and the blue sides. The pulse frequency change due to SPM is equal to:

$$\Delta\omega = \frac{\partial}{\partial t}\left(-\frac{\omega_0 \Delta n(t)}{c} z\right) = -\frac{\omega_0}{c} z \frac{\partial[\Delta n(t)]}{\partial t} \tag{3}$$

where z is the propagation distance, ω_0, the central angular frequency of the laser. In this case, the nonlinear refractive index is given by:

$$\Delta n(t) = n_2 I(t) - \frac{4\pi e^2 N_e(t)}{2 m_e \omega_0^2}. \tag{4}$$

Here, $n_2 I(t)$ is the Kerr nonlinear refractive index of the neutral gas, $I(t)$ being the intensity. The last term is the plasma contribution, where $N_e(t)$ is the generated electron; e and m_e are the charge and mass of an electron, respectively. We note that the electron-ion recombination time is normally much longer than the femtosecond time scale of the pulse. Hence, the generated plasma could be considered as static during the interaction with the pulse. Since the front part of the pulse always sees the neutral, from Eqs. (3) and (4), without the plasma contribution,

$$\Delta\omega = -\frac{\omega_0 z}{c}\frac{\partial[\Delta n(t)]}{\partial t} = -\frac{\omega_0 z}{c} n_2 \frac{\partial I(\text{front part})}{\partial t} < 0\,. \tag{5}$$

The last inequality in Eq. (5) arises because the front part of the pulse has a positive temporal slope whose value ranges continuously between zero and a maximum value; hence, the front part of the pulse contributes principally to red (Stokes) shift/broadening. But the back part of the pulse should also see the neutral since the medium is only partially ionized. SPM in the neutral would lead to a blue shift/broadening but this blue shift is masked by the stronger blue shift/broadening due to SPM in the plasma together with the eventual SPM due to the very steep descent of the back part of the pulse (i.e. self-steepening) [17,25].

This so-called self-steepening in the course of the propagation of a powerful femtosecond pulse is the consequence of a continuous spatio-temporal self-transformation process of the pulse during propagation. The central slice of the pulse with the highest intensity where ionization occurs would propagate with a velocity c/n where $n = n_0 + \Delta n_{Kerr} - \Delta n_p$. Here, n, is the total index of refraction, n_0, Δn_{Kerr} and Δn_p are the indices of refraction of the neutral air, the nonlinear Kerr index and the index of the plasma, respectively. At the intensity clamping position, $\Delta n_p = \Delta n_{Kerr} = n_2 I$. This focusing central slice with intensity clamping would thus have an index of refraction $n_c = n_0$; it would propagate faster than the front part of the pulse which sees an increase of the index of refraction due to the nonlinear contribution (Kerr nonlinear index) only $n_f = n_0 + \Delta n_{Kerr}$; i.e. no plasma generation yet. Now the back part of the pulse sees a weak plasma generated by the peak of the pulse. The index of refraction of this plasma zone is the combined values of the neutral and the weak plasma; i.e. $n_b = n_0 + (\Delta n_{Kerr})_b - \Delta n_p$; here $(\Delta n_{Kerr})_b < \Delta n_p$ because the intensity of this back slice is weaker than the clamped intensity while the plasma is left behind by the clamped intensity. Hence, $n_b < n_c < n_f$; i.e. the back part of the pulse would propagate faster than the front part of the pulse. Soon, the back part would almost catch up with the front part resulting in a steep rise in intensity at the back part. SPM is proportional to the derivative of this part of the pulse; hence, a very large blue shift according to Eq. (6):

$$\Delta\omega = \frac{\omega_0 z}{c} n_2 \frac{\partial I(\text{very steep back part with negative slope})}{\partial t}. \tag{6}$$

The propagation distance *z* also plays a role in both the red and blue broadening (see Eqs. (5) and (6)); thus, during experimental observations, the spectral broadening of the pulse develops progressively as the propagation distance increases. Both experiment and numerical simulation [17,18,25] show similar broadening. The central part of the pattern of Fig. 1 is an example of such frequency broadening from the pump at 800nm towards the blue side across the whole visible frequency range; hence, it appears white at the center. It is what we call the self-transformed white light laser pulse (ref. [3,18]).

FIG. 1. A chirped white light laser pattern. It started from a 5 mJ/45 fs Ti-sapphire laser pulse (at around 800 nm). After propagating a distance of 25 m in air, it turns into a white light laser pulse. Note the central white spot and the rainbow colored rings extending from red (longer wavelength) near the center to blue (shorter wavelength) at the outside.

The colorful rings in Fig. 1 are another manifestation of self-phase modulation in the radial direction (conical emission; for a general review, see also [24]). The descriptions of SPM in the previous section have considered only the wave vector k_z. However, the laser pulse front is curved at the self-focal zone. It contains a transverse part of the wave vector. In a normally spherically symmetric pulse front, the general wave vector $\vec{k}$ is given by:

$$\vec{k} = k_z\hat{z} + k_r\hat{r} = k_{z0}\hat{z} + \Delta k_z\hat{z} + k_{r0}\hat{r} + \Delta k_r\hat{r} \qquad (7)$$

where the initial wave vectors contain a subscript zero. $\hat{z}$ is a unit vector in the propagation direction; $\hat{r}$ is a unit vector transverse to $\hat{z}$. In the plane wave approximation described above, we have considered only the *z*-components. They are:

$$\Delta k_z\hat{z} = -\frac{\omega\Delta n}{c}\hat{z} = \int_0^t \frac{(\Delta\omega)}{z}dt\,\hat{z}$$

$$= \begin{cases} -\dfrac{\omega_0}{c}n_2\displaystyle\int_0^t \frac{\partial I(\text{front part})}{\partial t}dt\,.\hat{z} < 0 \text{ (in neutral gas)} \\ +\dfrac{2\pi e^2}{cm_e\omega_0}\displaystyle\int_0^t \frac{\partial N_e}{\partial t}dt\,.\hat{z} > 0 \qquad \text{(in plasma)} \end{cases} \qquad (8)$$

$$= \begin{cases} -\dfrac{\omega_0}{c}n_2\displaystyle\int_0^z \frac{\partial I(\text{front part})}{\partial z}dz\,.\hat{z} < 0 \text{ (in neutral gas)} \\ +\dfrac{2\pi e^2}{cm_e\omega_0}\displaystyle\int_0^z \frac{\partial N_e}{\partial z}dz\,.\hat{z} > 0 \qquad \text{(in plasma).} \end{cases} \qquad (9)$$

We see that from Eqs. (8) and (9), the temporal rate of change has been transformed into a spatial rate of change by recognizing that $z = ct$. Fig. 2(a) gives a schematic relationship of these waves vectors. $\Delta k_z\hat{z}$ (plasma), being positive, is in the same direction as that of the original vector $k_{z0}\hat{z}$ while $\Delta k_z\hat{z}$ (neutral), being negative, is in the opposite direction to that of $k_{z0}\hat{z}$.

Eq. (9) shows that the spatial gradient of the electron density gives rise to a blue shift of the frequency in the *z*-direction (plane wave approximation). Since electrons are generated in the 3-D self-focal volume, electron density gradients show up in all directions; i.e. in both the *z*- and the *r*-directions. In the *r*-direction, the electron density gradient would give rise to a spatial divergence of the radiation. Thus, the wave vector, $\Delta k_r\hat{r}$ (plasma), which is in the direction of $k_{r0}\hat{r}$, would make this blue shifted radiation diverging into a ring as shown by the vector diagram in Fig. 2(b). The larger the electron density gradient is, the larger will be the wave vector $\Delta k_r\hat{r} \sim \dfrac{\partial N_e}{\partial r}\vec{r}$ and the blue shift (Eqs. (3) and (9)). The radial electron density gradient varies continuously from zero to a maximum value. From Fig. 2(b), the divergence of the resultant vector $\vec{k}$ will be larger when the electron density gradient is larger. Hence, rainbow-type colored rings are generated around the central white spot; the larger the frequency shift is (i.e. the shorter the shifted wavelength is), the larger the divergence will be. The rings in Fig. 1 are thus explained. The frequency shift due to the neutrals would not give rise to rings because the wave vector $\Delta k_r\hat{r}$ (neutral) points in the opposite direction of $\vec{k}_{r0}$; i.e. it tends to reduce the divergence of the wave.

III. REFOCUSING

The filament could be visualized by recording the fluorescence signals emitted through the plasma recombination process. The top panel in Fig. 3 shows a typical picture taken with an ICCD (intensified CCD) camera from the side of the filament which is the result of the propagation of a 45 fs Ti-sapphire laser pulse in air in a clean laboratory environment. The fine line of light comes mainly from the fluorescence of nitrogen molecules [26-28] with non-uniform intensity along the propagation axis. The diameter of the line is less than 100 microns. This is a manifestation of a single filament; but the line is not uniform. It shows a series of brighter sections separated by darker zones; i.e. the laser pulse undergoes multiple re-focusing generating a few filaments along the same propagation axis.

The re-focusing phenomenon is contributed by the energy reservoir. If we use a sensitive burn paper to intercept the pulse at different positions of the propagation, we shall observe a pattern similar to the one shown in the bottom left panel in Fig. 3. The central black spot is the so-called self-focal spot and the succession of such spots (self-foci) along the propagation axis gives rise to the perception of a filament. It looks as if there were only a single filament (a series of hot spots) along the propagation axis; but in fact, there is a lot more radiation energy stored in the surrounding area which is normally not observed or omitted in many experiments. We call this surrounding zone the background reservoir [15,18-20].

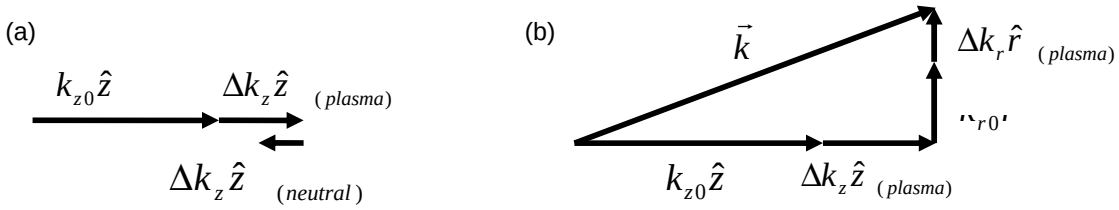

FIG. 2. Illustration of the various wave vectors of a spherical wave front in the self-focal region. (a) All the possible wave vectors in the propagation z-direction are shown. (b) Illustrating the transverse part of the wave vector.

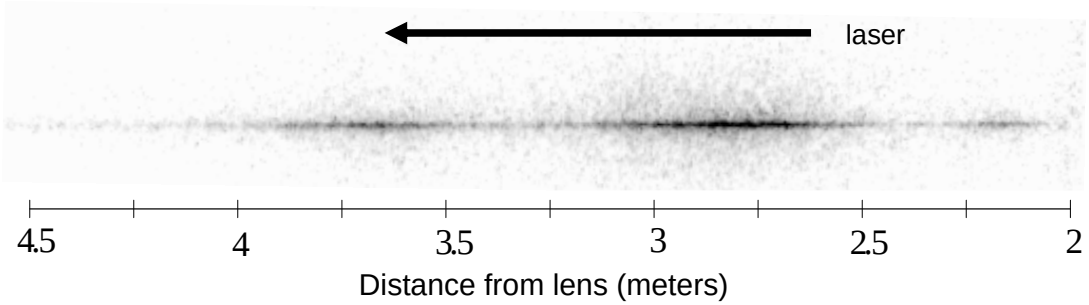

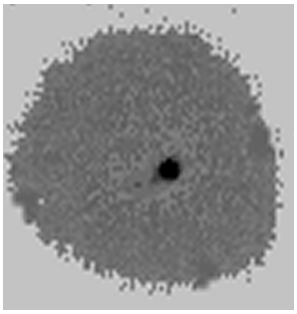

FIG. 3. (Top): Filament measured in air using an ICCD camera. The filament is produced after a f = 5 m focusing lens. The wavelength of the Ti-sapphire laser pulse was centered around 800 nm; the pulse energy was 13 mJ; the transform limited pulse length was 45 fs (FWHM). The diameter of the filament is of the order of 100 microns.
Left: Burn pattern of the cross section of the 'filament'

To understand how energy reservoir (or the slice-by-slice self-focusing picture) induces re-focusing, in Fig. 4 we plot the filament energy, defined as the energy contained in a 150-micron diameter to the total pulse energy as a function of the propagation distance [17]. Initially due to self-focusing more energy of the pulse is channeled into the core region until there is enough plasma generated to stop the self-focusing process, and the beam starts to defocus. However, the defocusing is stopped and the pulse refocuses again, which can be seen as the second peak in the filament energy. This process can repeat itself many times resulting in multiple self-focusing collapses, which is apparent from Fig. 4 as a weak third peak in the filament energy. The refocusing of the pulse channels energy from the background reservoir back into the core of the beam and thus represents the process in which energy is exchanged between the core and the outer part (reservoir) of the beam. This is one of the important physical mechanisms of the long-range propagation and filament formation in air.

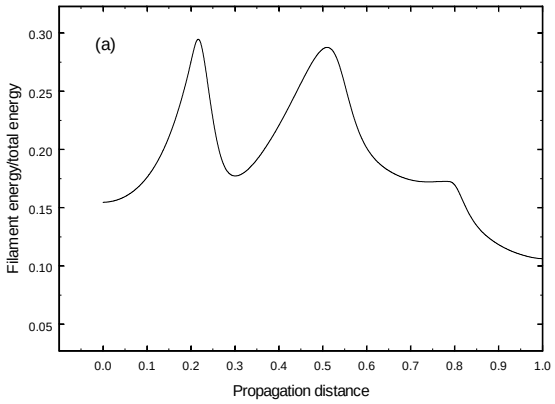

FIG. 4. The filament energy contained in a cylinder of 150 μm diameter

IV. MULTIPLE FILAMENTATION COMPETITION AND SELF-GUIDED HOT LIGHT PULSE

The above description pertains to a single filament arising from one higher intensity ('warm') zone of a pulse. Very often, the pulse front is not uniform either because of inherent imperfection of the laser itself or because of external perturbation such as turbulence in air (see for example, [29]) or the passage through a window [30] etc. The basic principle of multiple filamentation [31] is the formation of more than one 'warm' zone on the wave front. Each 'warm' zone will undergo self-focusing when the pulse propagates in air as if it were an independent pulse. But these 'warm' zones are not independent from one another because they all try to feed energy from the whole pulse's back ground reservoir into their own self-foci. This constitutes a competition for energy [32-35]. The physics of multiple filament competition is essentially field re-distribution inside the pulse during propagation. It consists of two inter-related scenarios. One scenario is linear field interference inside the pulse during propagation and self-deformation through the optical medium. The other is nonlinear field re-distribution due to nonlinear propagation effects.

In the first scenario, consider first a 'warm' zone as being a single pulse. When a slice of the 'warm' zone self-focuses towards a high intensity spot, ionization occurs and the intensity is clamped. With further propagation, the slice will diverge outwards becoming a conical wave which interferes with the background field (a quasi plane wave) giving rise to concentric rings around the self-focus [30,36]. When two adjacent 'warm' zones self-focus into two near-by self-foci, the two sets of rings (or rather, the two conical waves and the background quasi-plane wave) will interfere giving rise to a star-like pattern [30]. This is shown in Fig. 5 in which two filaments/hot spots (one strong and one weak) resulting from the propagation of a non-uniform 14 mJ 800 nm Ti-sapphire laser pulse in air interfere forming such a star-like structure. When more than two near-by filaments interfere, the resultant field would give rise to more complicated structures with more new 'warm' zones which would undergo self-focusing again during further propagation. New 'children' filaments are thus formed at new positions both along the propagation axis and on the cross sectional surface [34].

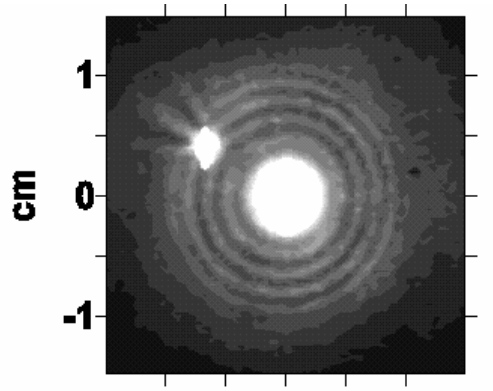

FIG. 5. Interference of two filaments: one weak, one strong.

However, if the 'warm' zones or filaments are far apart, interference would be too weak to form new and sufficiently 'warm' zones for self-focusing. This would constitute the second scenario in which the initial 'warm' zones would each go its own way as if they were independent. During the propagation, the nonlinear self-focusing effect would help each of the 'warm' zones to 'pull' the field towards its own self-focus as if each filament 'sucks' energy from the background reservoir. The consequence of this competition for energy from the same background reservoir would be such that the

filaments do not have enough energy to develop fully into mutual filaments.

Such competition for energy would also take place in the first scenario with filaments adjacent to one another but in a more constructive way because the filaments are close to one another. Apart from creating 'children' filaments, the central bunch of filaments would collectively 'suck' energy from the background reservoir towards them as if they were one single filament. The consequence of this latter case is that all these filaments become mature almost at the same time over a short distance of propagation. In air, in such a short distance, the nitrogen fluorescence signal is very strong. After this short distance, the children filaments take over but will not be as strong as before [35].

These two scenarios were observed in recent experiments [34,35], in which the nitrogen back scattered fluorescence (BSF) from long filaments in air was measured using a LIDAR (laser radar) technique. It was found that with a beam diameter of about 25 mm ($1/e^2$ of fluence) over which the multiple 'warm' zones were sufficiently far apart, the back scattered fluorescence from the generated multiple filaments had a huge fluctuation. For the same input laser peak power of about 1 Terawatt (TW, or 10^{12} W), the fluorescence signal sometimes came from the full propagation length of 100 m (Fig. 6(a)) but sometimes, there was very little after about 20 m of filamentation and sometimes, nothing at all (Fig. 6(b)). However, if the beam diameter is made smaller while keeping the distribution of 'warm' zones roughly the same; i.e. forcing the generated hot spots to be closed to one another, we could detect back scattered fluorescence from the full 100 m propagation length and beyond up to 500 m through extrapolation for all laser shots; also, in the first 10 m, the fluorescence intensity was more than 100 times stronger than the case of larger diameter (25 mm) beam [35].

In another laboratory experiment, we observed that the diameter of a 45 fs, 1 TW laser pulse's pattern at the original 800 nm wavelength remains practically constant after 100 m of propagation. As shown in Fig. 7, the initial pulse pattern contained a lot of 'warm' zones (Fig. 7(a)) and the final pattern still contained a lot of hot spots at the end of the propagation path in the corridor of 100 m (Fig. 7(b)). However, when the pulse length was lengthened (positively chirped) to about 200 ps, everything else being identical, the diameter at 100 m was more than three times larger than the initial diameter. The reason for the quasi-maintenance of the beam diameter is due to slice-by-slice self-focusing. Each self-focusing of a 'warm' zone means that the energy of the pulse is 'sucked' towards the self-focal region and then it is released back to the background reservoir after the self-focus. Successive slices would repeat the same process. When there are many self-foci (multiple filamentation), each of the self-foci contributes to 'sucking' energy from the background reservoir towards their respective focal zone and releasing it back to the reservoir. So long as the power in a 'warm' zone is above the critical power for self-focusing, this 'sucking' process would take place and slow down the linear diffraction of the pulse. We call this pulse a 'self-guided hot light pulse' [37]. This is perhaps another indication that the pulse could propagate very far in air and still might give rise to high intensities in the pulse. This optimism is indicated by recent experiments showing that the filament end at a distance of about 2 km in the atmosphere using 3 TW pulses [38]. A long pulse laser cannot do so.

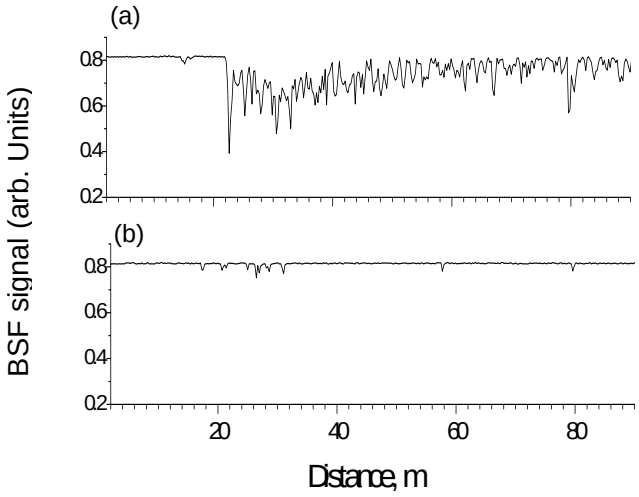

FIG. 6. Back scattered fluorescence in air as a function of distance. Both (a) and (b) are under identical laser conditions: 800 nm, 46 mJ, 42 fs.

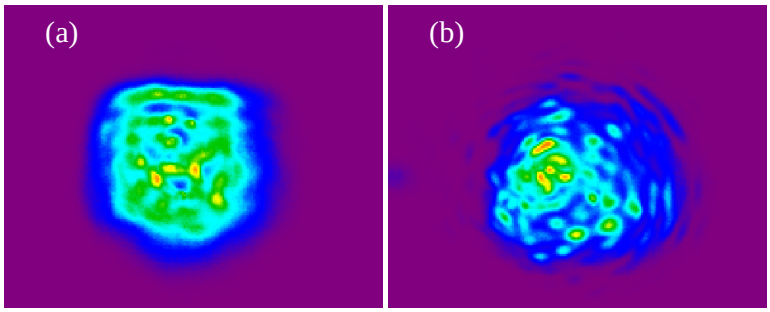

FIG. 7. Patterns of a 45 fs/50mJ Ti-sapphire laser pulse in air after propagating 20 m (a) and 80 m (b). The wavelength of the patterns is around 800nm which is the original wave length of the pulse.

Because all practical laser pulse front is not perfect, multiple filamentation at high pulse energy is unavoidable. Also, turbulence in air would also lead to the random change of the wave front for long distance propagation. A question is how one could control multiple filamentation [39]. This challenge would have many practical consequences. For example, one would like to overcome/make use of multiple filamentation and still able to generate strong filamentation at long distances into the atmosphere.

V. REMOTE-SENSING AND LIGHTENING CONTROL IN THE ATMOSPHERE

The filamentation of the femtosecond laser pulse in air results in a peak intensity of about 5 $\times 10^{13}$ W/cm^2, and the white light laser pulse's spectrum extends from the near UV (~350 nm) to the infrared (~4 microns) [17,40,41]. At the same time, an efficient third harmonic pulse at around 267 nm is generated inside the filament and it follows the fundamental self-focusing pulse 'faithfully' [41-44]. The recombination decay of the plasma column generates a weak but measurable electro-magnetic signal as well as THz pulses [45-49]. Some potential applications include making use of the back scattered white light as a source to measure pollutant absorption using the LIDAR technique. This was and is still being exploited by the French and German consortium using the unique Teramobile [50]. It is conceivable also to use the LIDAR technique to measure the back scattered fluorescence from the ionized and fragmented molecules inside the filaments in the path of propagation [51]. This latter technique together with the possibility of ASE type of gain in the signal [52] is being studied in the authors' laboratory. One could take advantage of the resulting plasma 'channel' left behind by filamentation and apply it to lightning control [4,53-56] and probably even artificial rain making [57].

VI. WRITING WAVEGUIDES IN GLASSES

During self-focusing of powerful fs laser pulses in bulk glass (fused silica or quartz), the free electrons generated in the conduction band will return back to the valence band through radiative and non-radiative transitions and through the formation of excitons followed by its self-trapping [58]. The relaxation of a self-trapped excitons leads to the formation of an intrinsic structural defect. If the transition were radiative, it would generate UV photons whose energy would be as large or larger than the band gap energy. Such photons would be re-absorbed by the electrons in the valence band and would finally turn into heating the local zone. Thus both radiative and non-radiative transitions would lead to a local heating of the glass material. We have observed that such heating leads to the melting of glass [59,60]. The ejected powder from glass surfaces shows beads of smooth and round (signs of melting) micron and sub-micron size particles observed under a scanning electron microscope. X-ray diffraction shows that using 1 kHz repetition rate 180 fs Ti-sapphire laser pulses to generate the powder, fused silica partially crystallizes into several types of high pressure SiO_2 crystals. However, only melting but no crystallization was observed in the case of quartz [59]. (Note that crystallization in fused silica is also another sign of melting because crystals can only be formed from hot liquid phase.) We attribute this to the higher thermal conductivity in quartz which quickly dissipates the heat between pulses so that no high pressure could be generated.

In 1996, Hirao's group [61] has discovered that fs laser pulses can write waveguides in fused silica. Since then, many groups studied different ways of writing waveguides. Our study indicates that melting and filamentation are responsible for the writing of good waveguide. Under certain focusing conditions, filamentation dominates the propagation. The local 'gentle' melted material inside the filament zone would cool down resulting in a uniform higher index of refraction. This would give rise to a good wave guide when the laser pulse is scanned through a linear zone

[62]. Much stronger focusing condition would merge the self-focus and the geometrical focus together and the ionization in this mixed zone would be stronger though still not strong enough to give a total breakdown. Nevertheless, a local small explosion would occur which would result in voids. Such void would not favor the formation of good waveguides [63].

VII. CONCLUSION

The fundamental physics of filamentation of a femtosecond laser pulse in transparent optical media has been well studied and is believed to be rather well understood. The principal idea of such filamentation is slice-by-slice self-focusing and it implies the idea of background reservoir. The qualitative physics of multiple filamentation is also known but from the practical point of view, there is this challenge of controlling them. There are many old and new challenging applications in the horizon. Recently many people are enter this field of research from the point of view of applications.

REFERENCES

[1] J. H. Marburger, Prog. Quant. Electr., **4**, 35 (1975).
[2] A. Brodeur, C. Y. Chien, F. A. Ilkov, S. L. Chin, O. G. Kosareva and V. P. Kandidov, Opt. Lett., **22**, 304 (1997).
[3] S. L. Chin, A. Brodeur, S. Petit, O. G. Kosareva and V. P. Kandidov, JNOPM, **8**, 121 (1999).
[4] H. Schillinger and R. Sauerbrey, Appl. Phys. B, **68**, 753 (1999).
[5] A. Talebpour, S. Petit and S. L. Chin, Opt. Commun., **171**, 285 (1999).
[6] S. Tzortzakis, M. A. Franco, Y. -B. André, A. Chiron, B. Lamouroux, B. S. Prade and A. Mysyrowicz, Phys. Rev. E, **60**, R3505 (1999).
[7] B. L. Fontaine, F. Vidal, Z. Jiang, C. Y. Chien, D. Comtois, A. Desparois, T. W. Johnston, J. -C. Kieffer, H. Pépin and H. P. Mercure, Physics of Plasma, **6**, 1615 (1999).
[8] C. Y. Chien, B. L. Fontaine, A. Desparois, Z. Jiang, T. W. Johnston, J. C. Kieffer, H. Pépin, F. Vidal and H. P. Mercure, Opt. Lett., **25**, 578 (2000).
[9] X. Mao, S. S. Mao and R. E. Russo, Appl. Phys. Lett., **82**, 697 (2003).
[10] Q. Sun, H. Jiang, Y. Liu, Z. Wu, H. Yang and Q. Gong, Opt. Lett., **30**, 320 (2005).
[11] J. Kasparian, R. Sauerbrey and S. L. Chin, Appl. Phys. B, **71**, 877 (2000).
[12] A. Becker, N. Aközbek, K. Vijayalakshmi, E. Oral, C. M. Bowden and S. L.Chin, Appl. Phys. B, **73**, 287 (2001).
[13] W. Liu, S. Petit, A. Becker, N. Aközbek, C. M. Bowden and S. L. Chin, Opt. Commun., **202**, 189 (2002).
[14] O. G. Kosareva, V. P. Kandidov, A. Brodeur and S. L. Chin, JNOPM, **6**, 485 (1997).
[15] M. Mlejnek, E. M. Wright and J. V. Moloney, Opt. Lett., **23**, 382 (1998).
[16] A. Chiron, B. Lamouroux, R. Lange, J. -F. Ripoche, M. Franco, B. Prade, G. Bonnaud, G. Riazuelo and A. Mysyrowicz, Eur. Phys. J. D, **6**, 383 (1999).
[17] N. Aközbek, M. Scalora, C. M. Bowden and S. L. Chin, Opt. Commun., **191**, 353 (2001).
[18] V. P. Kandidov, O. G. Kosareva, I. S. Golubtsov, W. Liu, A. Becker, N. Akozbek, C. M. Bowden and S. L. Chin, Appl. Phys. B, **77**, 149 (2003).
[19] M. Mlejnek, E. M. Wright and J. V. Moloney, IEEE J. of Quant. Electron., **35**, 1771 (1999).
[20] V. P. Kandidov, O. G. Kosareva and A. A. Koltuna, Quantum Electron., **33**, 69 (2003).
[21] F. Courvoisier, V. Boutou, J. Kasparian, E. Salmon, G. Méjean, J. Yu and J. -P. Wolf, Appl. Phys. Lett., **83**, 123 (2003).
[22] W. Liu, J. -F. Gravel, F. Théberge, A. Becker and S. L. Chin, Appl. Phys. B, **80**, 857 (2005).
[23] W. Liu, F. Théberge, E. Arevalo, J. -F. Gravel, A. Becker and S. L. Chin, Opt. Lett., Accepted (2005).
[24] R. W. Boyd, *Nonlinear Optics*, Academic Press, Boston (2003).
[25] A. L. Gaeta, Phys. Rev. Lett., **84**, 3582 (2000).
[26] A. Talebpour, M. Abdel-Fattah and S. L. Chin, Opt. Commun., **183**, 479 (2000).
[27] A. Talebpour, M. Abdel-Fattah, A. D. Bandrauk and S. L. Chin, Laser Physics, **11**, 68 (2001).
[28] A. Becker, A. D. Bandrauk and S. L. Chin, Chem. Phys. Lett., **343**, 345 (2001).
[29] S. L. Chin, A. Talebpour, J. Yang, S. Petit, V. P. Kandidov, O. G. Kosareva and M. P. Tamarov, Appl. Phys. B, **74**, 67 (2002).
[30] S. L. Chin, S. Petit, W. Liu, A. Iwasaki, M. -C. Nadeau, V. P. Kandidov, O. G. Kosareva and K. Y. Andrianov, Opt. Commun., **210**, 329 (2002).
[31] V. I. Bespalov and V. I. Talanov, JETP Lett., **3**, 307 (1966).
[32] M. Mlejnek, M. Kolesik, J. V. Moloney and E. M. Wright, Phys. Rev. Lett., **83**, 2938 (1999).
[33] S. A. Hosseini, Q. Luo, B. Ferland, W. Liu, N. Aközbek, G. Roy and S. L. Chin, Appl. Phys. B, **77**, 697 (2003).
[34] S. A. Hosseini, Q. Luo, B. Ferland, W. Liu, S. L. Chin, O. G. Kosareva, N. A. Panov, N. Aközbek and V. P. Kandidov, Phys. Rev. A, **70**, 033802 (2004).
[35] Q. Luo, S. A. Hosseini, W. Liu, J. -F. Gravel, O. G. Kosareva, N. A. Panov, N. Aközbek, V. P. Kandidov, G. Roy and S. L. Chin, Appl. Phys. B, **80**, 35 (2005).
[36] N. Aközbek, C. M. Bowden and S. L. Chin, Journal of Modern Optics, **49**, 475 (2002).
[37] W. Liu, S. A. Hosseini, Q. Luo, B. Ferland, S. L. Chin, O. G. Kosareva, N. A. Panov and V. P. Kandidov, NEW JOURNAL OF PHYSICS, **6**, 6 (2004).

[38] M. Rodriguez, R. Bourayou, G. Méjean, J. Kasparian, J. Yu, E. Salmon, A. Scholz, B. Stecklum, J. Eislöffel, U. Laux, A. P. Hatzes, R. Sauerbrey, L. Wöste and J. -P. Wolf, Phys. Rev. E, **69**, 036607 (2004).
[39] V. P. Kandidov, N. Akozbek, M. Scalora, O. G. Kosareva, A. V. Nyakk, Q. Luo, S. A. Hosseini and S. L. Chin, Appl. Phys. B, **80**, 267 (2005).
[40] J. Kasparian, R. Sauerbrey, D. Mondelain, S. Niedermeier, J. Yu, J. -P. Wolf, Y. -B. Andre, M. Franco, B. Prade, S. Tzortzakis, A. Mysyrowicz, M. Rodriguez, H. Wille and L. Wöste, Opt. Lett., **25**, 1397 (2000).
[41] F. Théberge, W. Liu, Q. Luo and S. L. Chin, Appl. Phys. B, **80**, 221 (2005).
[42] N. Aközbek, A. Iwasaki, A. Becker, M. Scalora, S. L. Chin and C. M. Bowden, Phys. Rev. Lett., **89**, 143901 (2002).
[43] N. Aközbek, A. Becker, M. Scalora, S. L. Chin and C. M. Bowden, Appl. Phys. B, **77**, 177 (2003).
[44] F. Théberge, N. Aközbek, W. Liu, J. -F. Gravel and S. L. Chin, Opt. Commun., **245**, 399 (2005).
[45] A. Proulx, A. Talebpour, S. Petit and S. L. Chin, Opt. Commun., **174**, 305 (2000).
[46] X. Wang, M. Krishnan, N. Saleh, H. Wang and D. Umstadter, Phys. Rev. Lett., **84**, 5324 (2000).
[47] S. A. Hosseini, B. Ferland and S. L. Chin, Appl. Phys. B, **76**, 583 (2003).
[48] G. Méchain, S. Tzortzakis, B. Prade, M. Franco, A. Mysyrowicz and B. Leriche, Appl. Phys. B, **77**, 707 (2003).
[49] S. Tzortzakis, G. Mchain, G. Patalano, Y. -B. Andr, B. Prade, M. Franco, A. Mysyrowicz, J. -M. Munier, M. Gheudin, G. Beaudin and P. Encrenaz, Opt. Lett., **27**, 1944 (2002).
[50] J. Kasparian, M. Rodriguez, G. Méjean, J. Yu, E. Salmon, H. Wille, R. Bourayou, S. Frey, Y. -B. André, A. Mysyrowicz, R. Sauerbrey, J. -P. Wolf and L. Wöste, Science, **301**, 61 (2003).
[51] J.-F. Gravel, Q. Luo, D. Boudreau, X. P. Tang and S. L. Chin, Anal. Chem., **76**, 4799 (2004).
[52] Q. Luo, W. Liu and S. L. Chin, Appl. Phys. B, **76**, 337 (2003).
[53] X. M. Zhao, J. -C. Diels, C. Y. Wang and J. M. Elizondo, IEEE J. of Quant. Electron., **31**, 599 (1995).
[54] S. L. Chin and K. Miyazaki, Jpn. J. Appl. Phys., **38**, 2011 (1999).
[55] H. Pépin, D. Comtois, F. Vidal, C. Y. Chien, A. Desparois, T. W. Johnston, J. C. Kieffer, B. L. Fontaine, F. Martin, F. A. M. Rizk, C. Potvin, P. Couture, H. P. Mercure, A. Bondiou-Clergerie, P. Lalande and I. Gallimberti, Physics of Plasma, **8**, 2532 (2001).
[56] M. Rodriguez, R. Sauerbrey, H. Wille, L. Wste, T. Fuji, Y. -B. Andr, A. Mysyrowicz, L. Klingbeil, K. Rethmeier, W. Kalkner, J. Kasparian, E. Salmon, J. Yu and J.-P. Wolf, Opt. Lett., **27**, 772 (2002).
[57] S. L. Chin, Physics in Canada, **60**, 273 (2004).
[58] S. S. Mao, F. Quéré, S. Guizard, X. Mao, R. E. Russo, G. Petite and P. Martin, Appl. Phys. B, **79**, 1695 (2004).
[59] V. Koubassov, J. F. Laprise, F. Théberge, E. Förster, R. Sauerbrey, B. Müller, U. Glatzel and S. L. Chin, Appl. Phys. B, **79**, 499 (2004).
[60] M. R. Kasaai, V. Kacham, F. Théberge and S. L. Chin, J. Non-Cryst. Solids, **319**, 129 (2003).
[61] K. M. Davis, K. Miura, N. Sugimoto and K. Hirao, Opt. Lett., **21**, 1729 (1996).
[62] N. T. Nguyen, A. Saliminia, W. Liu, S. L. Chin and R. Vallee, Opt. Lett., **28**, 1591 (2004).
[63] N. T. Nguyen, A. Saliminia, S. L. Chin and R. Vallée, Proceedings of SPIE, **5578**, 665 (2004).